

Article

A Novel NADP(H)-Dependent 7 α -HSDH: Discovery and Construction of Substrate Selectivity Mutant by C-Terminal Truncation

Yinping Pan ^{1,†}, Shijin Tang ^{1,†}, Minghai Zhou ¹, Fanglin Ao ¹, Zhuozhou Tang ¹, Liancai Zhu ^{1,2,*}, Deshuai Lou ³, Jun Tan ³ and Bochu Wang ^{1,*}

¹ Key Laboratory of Biorheological Science and Technology, Ministry of Education, College of Bioengineering, Chongqing University, Chongqing 400030, China; 201819021098@cqu.edu.cn (Y.P.); 20161902090@cqu.edu.cn (S.T.); minghaizhou@cqu.edu.cn (M.Z.); 20185603@cqu.edu.cn (F.A.); 20185647@cqu.edu.cn (Z.T.)

² Modern Life Science Experiment Teaching Center, College of Bioengineering, Chongqing University, Chongqing 400030, China

³ Chongqing Key Laboratory of Medicinal Resources in the Three Gorges Reservoir Region, School of Biological & Chemical Engineering, Chongqing University of Education, Chongqing 400067, China; louds@cque.edu.cn (D.L.); tanjun@cque.edu.cn (J.T.)

* Correspondence: zhuliancai@cqu.edu.cn (L.Z.); wangbc@cqu.edu.cn (B.W.)

† These authors contributed equally to this work.



Citation: Pan, Y.; Tang, S.; Zhou, M.; Ao, F.; Tang, Z.; Zhu, L.; Lou, D.; Tan, J.; Wang, B. A Novel NADP(H)-Dependent 7 α -HSDH: Discovery and Construction of Substrate Selectivity Mutant by C-Terminal Truncation. *Catalysts* **2022**, *12*, 781. <https://doi.org/10.3390/catal12070781>

Academic Editors: Jose M. Guisan, Antonio Zuorro and Yung-Chuan Liu

Received: 16 June 2022

Accepted: 11 July 2022

Published: 14 July 2022

Publisher's Note: MDPI stays neutral with regard to jurisdictional claims in published maps and institutional affiliations.



Copyright: © 2022 by the authors. Licensee MDPI, Basel, Switzerland. This article is an open access article distributed under the terms and conditions of the Creative Commons Attribution (CC BY) license (<https://creativecommons.org/licenses/by/4.0/>).

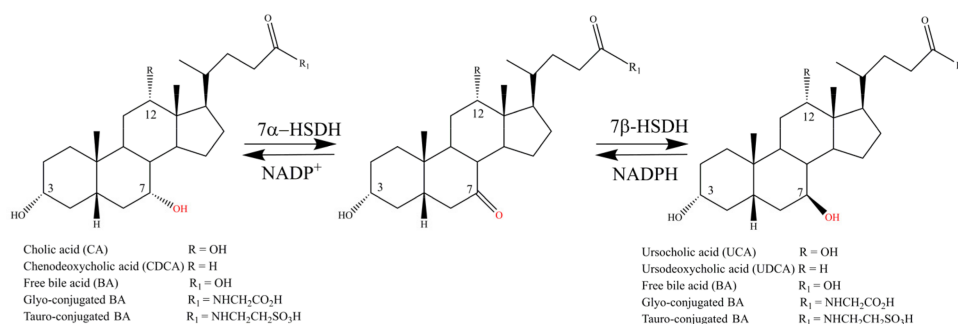
Abstract: 7 α -Hydroxysteroid dehydrogenase (7 α -HSDH) plays an important role in the biosynthesis of tauroursodeoxycholic acid (TUDCA) using complex substrate chicken bile powder as raw material. However, chicken bile powder contains 4.74% taurocholic acid (TCA), and a new by-product tauroursocholic acid (TUCA) will be produced, having the risk of causing colorectal cancer. Here, we obtained a novel NADP(H)-dependent 7 α -HSDH with good thermostability from *Ursus thibetanus* gut microbiota (named St-2-2). St-2-2 could catalyze taurochenodeoxycholic acid (TCDCA) and TCA with the catalytic activity of 128.13 and 269.39 U/mg, respectively. Interestingly, by a structure-based C-terminal truncation strategy, St-2-2 Δ C10 only remained catalytic activity on TCDCA (14.19 U/mg) and had no activity on TCA. As a result, it can selectively catalyze TCDCA in waste chicken bile powder. MD simulation and structural analysis indicated that enhanced surface hydrophilicity and improved C-terminal rigidity affected the entry and exit of substrates. Hydrogen bond interactions between different subunits and interaction changes in Phe249 of the C-terminal loop inverted the substrate catalytic activity. This is the first report on substrate selectivity of 7 α -HSDH by C-terminal truncation strategy and it can be extended to other 7 α -HSDHs (J-1-1, S1-a-1).

Keywords: 7 α -hydroxysteroid dehydrogenase (7 α -HSDH; St-2-2); St-2-2 Δ C10; C-terminal truncation; substrate selectivity; tauroursodeoxycholic acid

1. Introduction

Ursodeoxycholic acid (UDCA) and TUDCA, a taurine-conjugate derivative of UDCA, have been widely used to treat hepatobiliary diseases, including primary biliary cholangitis (PBC) [1], primary sclerosing cholangitis [2], biliary cirrhosis [3]. Several methods have been developed for the synthesis of TUDCA [4]. However, the use of organic reagents, such as diethylpyrocarbonate (DEPC), in chemical synthesis causes environmental pollution [5]. In vivo, the synthesis of TUDCA needs five steps (Figure S1). TCDCA is hydrolyzed to CDCA under the action of the bile acid hydrolase (BSH), then CDCA is converted into UDCA under the catalysis of 7 α -HSDH and 7 β -HSDH, and finally, UDCA is catalyzed into TUDCA by bile acid-COA ligase (BAL) and bile acid-N-acetyltransferase [6–8]. In vitro, TUDCA can be produced by a two-step enzymatic reaction using 7 α -HSDH and 7 β -HSDH as catalysts, which are mild, and environmentally friendly [9]. 7 α -HSDHs can catalyze the

C-7 α -position hydroxyl dehydroxylation reaction of CA or CDCA and their taurine or glycine conjugates, such as TCA, TCDCA, glycocholic acid (GCA), and glycochenodeoxycholic acid (GCDCA) to form keto groups, then 7β -HSDHs catalyze the reduction of the keto group to β -OH, realizing the epimerization of 7-OH configuration inversion, and the coenzyme NADP(H) is added to realize the reaction cycle (Scheme 1) [10]. Ji et al. pointed out that chicken bile powder could be selected as the substrate for biosynthesis of TUDCA owing to its high content of TCDCA (about 42.58%), turning waste into treasure [11,12]. However, chicken bile powder contains 4.74% TCA, and a new by-product TUCA could be produced, resulting in purification difficulties and lower production of TUDCA. Therefore, the lack of 7α -HSDH that specifically catalyzes TCDCA hinders TUDCA biosynthesis from chicken bile powder.



Scheme 1. Epimerization of CDCA or CA into UDCA or UCA by the sequential use of 7α -HSDH and 7β -HSDH.

7α -HSDHs belong to short-chain dehydrogenases/reductases (SDRs) sharing a Rossmann fold-type domain [13]. According to the study of the three-dimensional structure and function of *Escherichia coli* (PDB code: 1AH, 1FMC, 1AHI), *Brucella melitensis* (PDB code: 3GAF), and *Clostridium absonum* (PDB code: 5EPO), the C-terminal is highly unconservative and structurally diverse. Proceeding from the sequence–structure–function relationship, protein engineering strategies have been used for engineering enzymes to study catalytic efficiency [14], cofactor specificity [15,16], thermostability [17], substrate specificity [18], and so on. Kim et al. [19] proposed a systematic strategy for key points screening based on the sequence–structure–function relationship and they found the determination of the catalytic efficiency of Arylacetonitrilase was Phe 140. Gao et al. [20] studied the dual substrate specificity of LreNo through homology modeling and structure analysis. Gly155, Ser179, and His184 of LreNo were crucial for NADPH recognition. Protein engineering strategies have also been used to modify hydroxysteroid dehydrogenases. Liu et al. [21] found that, compared with the wild type, single-site mutation I258M of *B. melitensis* 7α -HSDH had 21.8-fold higher k_{cat}/K_m , 2.0-fold lower K_m value with NAD⁺, and increased the half-life from 20.8 to 31.1 h at 30 °C. Huang et al. [22] designed a Q255L/C260S mutant, which had 5.5-fold higher specific activity and 100 mM substrate tolerance of CA 7α -HSDH. Dhagat et al. [23] reported that Y224D mutation in mouse 3(17) α -HSDH (AKR1C21) had 80-fold K_m reduced and completely reversed the 17α -stereospecificity of the enzyme. Besides, L308V mutation in human 20α -HSDH (AKR1C1) improved the catalytic efficiency of the two substrates [24]. Furthermore, removal of 8, 14, and 17 amino acids of the C-terminal region of CA 7α -HSDH, respectively, meant the activity could not be detected [25]. It showed that the C-terminal region was essential for the catalytic activity of CA 7α -HSDH. However, there has been no report on whether C-terminal modification can reverse catalytic activity towards different substrates. Recently, Kim et al. [26] reported the crystal structure of an apo 7α -HSDH and revealed that the C-terminal region covered the substrate-binding site and hindered the substrate from entering the substrate-binding site of the enzyme, which gave us an incentive to study the role of the C-terminal in 7α -HSDH substrate selectivity. What is more, due to being more often exposed to solvents resulting in non-covalent bonds placing fewer restrictions on adjacent residues, the terminal region of proteins was generally more

flexible than other functional regions [27]. Therefore, it is theoretically possible to achieve substrate selectivity by appropriate modification of the C-terminal residues.

In this study, we obtained a novel NADP(H)-dependent 7 α -HSDH (St-2-2) and cloned five 7 α -HSDH (St-2-2) genes truncated at the C-terminal domain. Fortunately, we obtained the mutant without activity on TCA, but with activity on TCDCA, and explained the mechanism of substrate selectivity by structure analysis and MD simulation. In addition, it was confirmed that the C-terminal truncation strategy could be extended to other 7 α -HSDHs (J-1-1, S1-a-1). This finding not only provides mutant 7 α -HSDHs for the biosynthesis of TUDCA using chicken bile powder as raw material, but also provides a new strategy for future works involving the design of the C-terminal region of hydroxysteroid dehydrogenase.

2. Results

2.1. Cloning, Expression, and Purification of St-2-2

Using known 7 α -HSDHs as templates to search the gene functional annotation and datasets of the predicted Open Reading Frames (ORFs), we successfully cloned and expressed a novel 7 α -HSDH gene (named St-2-2 gene) containing 789 base pairs coding for a novel protein of 262 amino acids. The 7 α -HSDH gene fragment was amplified by PCR from metagenomic DNA. Agarose electrophoresis proved that the DNA fragment contained about 789 bp. The PCR fragment was recombined with pGEX-6p-2 and expressed in *E. coli* BL21(DE3). The recombinant protein contained GST-tag for purification and PreScission Protease was used to excise the GST tag from it. The molecular mass of the 7 α -HSDH gene protein was verified by SDS-PAGE gel (Figure 1A), gel filtration (ÄKTA™ prime plus) (Figure 1A,B), and mass spectrometry (Figure 2C). What is more, according to gel filtration, St-2-2 had a native size of 113 kDa, supposed to be a tetramer in solution. However, CA 7 α -HSDH was dimer and tetramer coexisting [28], and St-2-1 existed as a dimer [29].

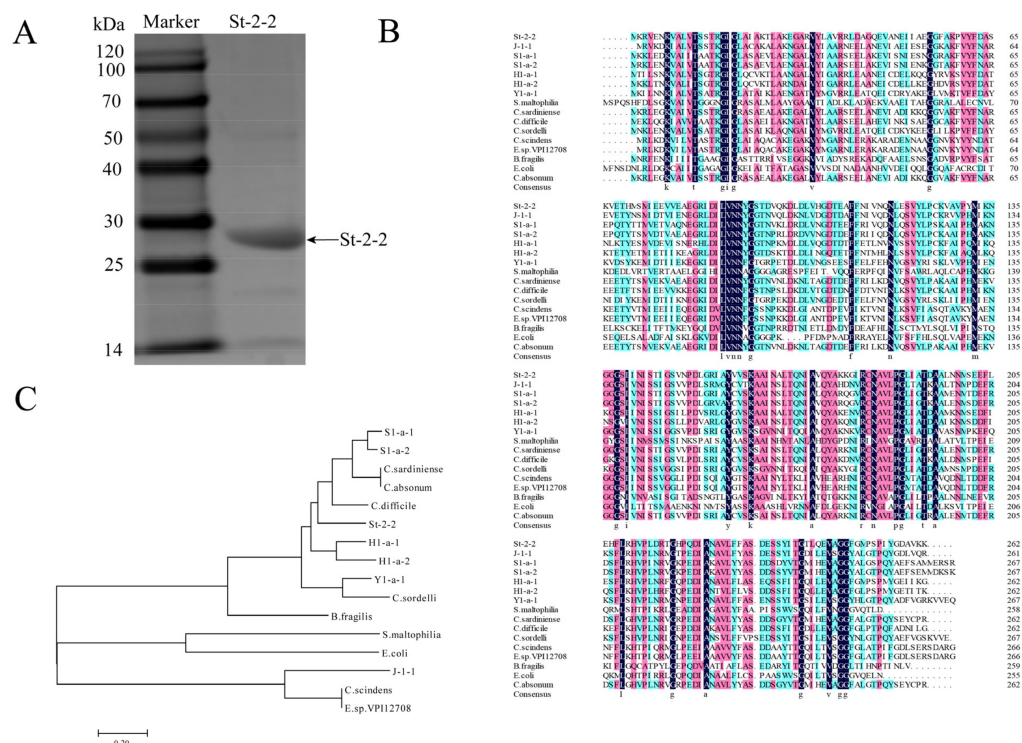


Figure 1. Identification of St-2-2. (A) SDS-PAGE analysis of the expression and purity of St-2-2 (loading 10 μ L, 1.5 mg/mL). (B) The homology alignment of the amino acid sequence of St-2-2 with other 7 α -HSDHs. (C) Phylogenetic tree based on the alignment of 7 α -HSDHs protein sequences.

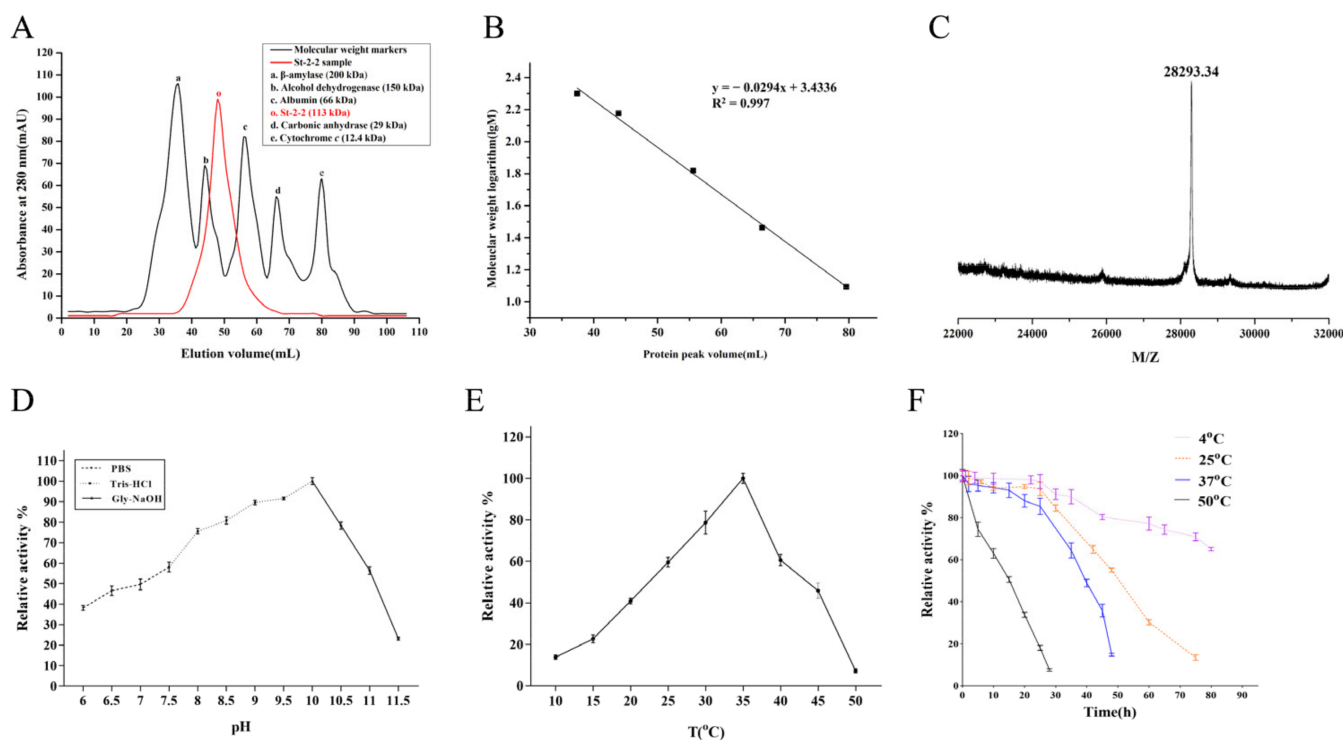


Figure 2. Characterization of St-2-2. (A) Elution curve of standard protein and St-2-2. (B) Standard curve. (C) Mass spectrometry. (D) Optimum pH for St-2-2. (E) Optimum temperature for St-2-2. (F) Thermostability of St-2-2.

2.2. Sequence Alignments and Phylogenetic Analysis

An amino acid sequence alignment of 7 α -HSDHs (J-1-1, H1-a-1, H1-a-2, S1-a-1, S1-a-2, Y1-a-1) from our previous work, involving nine known 7 α -HSDHs, including those from *Stenotrophomonas maltophilia* (GenBank: KRG42928.1) [30], *Clostridium sardiniense* (GenBank: AET80685.1) [9], *Clostridium difficile* (GenBank: CAJ66880.1, putative) [31], *Clostridium sordelli* (GenBank: L12058.1) [32], *Clostridium scindens* (GenBank: AAB61151) [33], *Eubacterium* sp. VPI 12708 (GenBank: M58473.1) [34], *Bacteroides fragilis* (GenBank: AF173833.2) [35], *Escherichia coli* (GenBank: ACI83195.1) [36], *Clostridium absonum* (GenBank: AF173833.2) [4], and St-2-2 were performed using “DNAMAN” software (Figure 1B). Sixteen 7 α -HSDHs sequences showed a high homology of 63.09%. The sequence clearly showed the conserved domains in the primary structure of 7 α -HSDHs. The N-terminal Gly-X-X-X-Gly-X-Gly sequence [37] was one of the conserved domains that characterized the cofactor-binding motif. There were three highly conserved active sites, Thr145-Tyr158-Lys162 constituting a catalytic triad of St-2-2. Thr145 immobilized the C7-OH of TCDCA by hydrogen bond, stabilizing the transition state of the substrate reaction and the correct orientation of the substrate in the binding pocket, while the protonated side chain (NH³⁺) of Lys162 interacted with nicotinamide ribose hydroxyl groups (2',3'-OH) and hydrogen bonds formed. Deprotonation of Tyr158 controlled the progress of the reaction (Figure S3).

In addition, the C-terminal amino acids were found to be variable in length and highly non-conserved. Based on the alignments, the homology tree (Figure 1C) showed that St-2-2 belonged to the same subgroup as *Clostridium difficile*, *Clostridium absonum*, *Clostridium sardiniense*, S1-a-1, S1-a-2. According to these results, St-2-2 was identified as a member of the SDRs family.

2.3. Optimum pH, Optimum Temperature, and Thermostability of St-2-2

Between pH 5.0–10.0, the activity of St-2-2 increased with increase of pH. However, the activity gradually decreased from pH 10.0 to pH 12.0. The results showed that the

optimum pH of St-2-2 was 10.0, indicating that St-2-2 was a basophilic enzyme (Figure 2D). An alkaline environment was conducive to the dissolution of substrates. From 10 °C to 35 °C, the activity of St-2-2 increased rapidly with a maximum at 35 °C, then decreased rapidly from 35 °C to 50 °C, due to protein denaturation. Thus, the enzyme was mesophilic (Figure 2E). St-2-2 was relatively stable at 4 °C, and its activity remained 87.9% after 48 h incubation. When St-2-2 was treated at 37 °C for 30 h, the activity of St-2-2 remained 66.5% (Figure 2F). While S1-a-1 and Y1-a-1 completely lost their activity at 37 °C for 30 h. The residual activities of S1-a-2, H1-a-1, H1-a-2 were 51.2%, 38.9%, 40.1%, respectively, after enzymes were treated at 37 °C for 30 h [38]. These results indicated that the thermostability of St-2-2 at 37 °C was significantly better than for the 7 α -HSDHs we found before. These results indicated that St-2-2 is a promising candidate for the industrial synthesis of TUDCA.

2.4. Structure Modeling and Target Mutation Identification

Structure-based modification is an important strategy for protein improvement as it takes advantage of protein structure analysis. The higher the amino acid sequence identity between the target protein and templates, the higher the accuracy of the prediction model. St-2-2 was modeled by using *Clostridium absonum* 7 α -HSDH (PDB ID: 5EPO, 64.34% identity) as a template. The C-terminal truncation strategy was proposed according to the following steps. Firstly, based on the primary sequence alignment, it was found that the length of the C-terminal amino acid was different and highly non-conservative. Secondly, compared with 7 α -HSDHs, which were crystal resolved, St-2-2 had an additional α -helix structure (Ile255-Tyr256-Gly257-Asp258-Ala259-Val260-Lys261-Lys262) (Figure S2). It was found that the C-terminal α -helix was not covered above the active cleft, and extended outward. The C-terminal α -helix and loop formed a specific spatial arrangement and were far from the active pocket (>5 Å) [25]. Lou et al. [39] also found that CA 7 α -HSDH had an extra α -helix at C-terminal which had a great influence on the catalytic activity of CA 7 α -HSDH. In contrast, the substrate-binding site of apo *Eco*-7 α -HSDH was blocked by the C-terminal loop, which might prohibit nonspecific hydrophobic molecules from entering [26]. Finally, based on the above sequence–structure–function relationship analysis, although the C-terminal was far from the active center, the wobbling of its tail might affect the entry and exit of the substrate. Therefore, the effect of C-terminal amino acids on the catalytic activity of St-2-2 on different substrates was explored by C-terminal truncation.

2.5. Effects of C-Terminal Domain Truncation of St-2-2 on Its Activity and Substrate Selectivity

7 α -HSDHs are generally known to contain N-terminal and C-terminal domains. In this study, it was found that the C-terminal domain played an important role in the activity and substrate selectivity of St-2-2. The catalytic activities of St-2-2 on TCDCA, GCDCA, TCA, and GCA were 128.13, 153.73, 269.39, and 175.88 U/mg. The catalytic activities of wild-type St-2-2 on CDCA-conjugated bile acids were lower than that of CA-conjugated bile acids. However, we found that mutant St-2-2 Δ C10 had no activity on TCA and GCA, but the activity on TCDCA and GCDCA remained 14.19 U/mg and 22.77 U/mg, respectively (Figure 3A). The catalytic efficiency (k_{cat}/K_m) of St-2-2 Δ C10 remained 0.5% of St-2-2, indicating that the C-terminal domain of St-2-2 contributed to substrate affinity (Table 1).

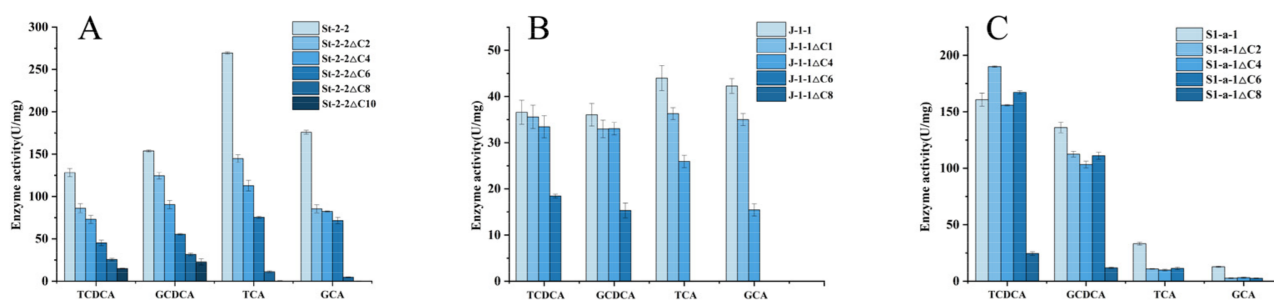


Figure 3. Effects of C-terminal truncation on substrate selectivity. Catalytic activities of (A) St-2-2, (B) J-1-1, (C) S1-a-1 and their mutants on TCDCA, GCDCA, TCA, and GCA.

Table 1. The kinetic parameters of the purified 7α -HSDHs.

Enzyme	Substrate	V_{max} (U/mg)	K_m (mM)	K_{cat} (S^{-1})	k_{cat}/K_m
St-2-2	TCDCA	152.85 ± 7.34	0.2 ± 0.01	102.34 ± 3.62	511.70
St-2-2 Δ C10	TCDCA	22.17 ± 2.12	3.97 ± 0.15	10.42 ± 0.09	2.62
J-1-1	TCDCA	387.14 ± 6.51	0.10 ± 0.01	192.86 ± 0.93	1872.40
J-1-1 Δ C6	TCDCA	56.18 ± 1.91	2.59 ± 0.03	27.08 ± 0.21	10.46
S1-a-1	TCDCA	369.23 ± 3.87	0.13 ± 0.01	236.54 ± 5.15	1791.95
S1-a-1 Δ C8	TCDCA	51.81 ± 3.13	2.04 ± 0.11	24.97 ± 3.11	12.23

Each value was calculated from triplicate experiments. \pm means standard deviations.

2.6. MD Simulation and Structural Analysis

St-2-2 has a complex C-terminal structure. From the quaternary structure (Figure 4A), the direct interaction between the two subunits in the diagonal direction was mediated through the C-terminal, with a diagonal A (green), B (blue) two subunits, for example, Ser253, Pro254, Asp258 of subunit A and Pro151/Asp152, His211, His211 of subunit B formed hydrogen bonds, respectively, while Tyr256 of subunit A and Pro213 of subunit A formed hydrogen bonds and vice versa. Compared to the wild type, St-2-2 Δ C8 had only two hydrogen bonds broken, while St-2-2 Δ C10 had five hydrogen bonds broken. With the number of hydrogen bonds reducing, the catalytic activity of the mutants decreased.

As for the secondary structure in St-2-2 Δ C10, the C-terminal α -helix was completely lost. The contents of each secondary structure of wild-type St-2-2 and mutants changed significantly (Figure 4B). Compared with WT, the α -helix of St-2-2 Δ C10 was reduced by 28.84%, and β -sheet St-2-2 Δ C10 increased by 21.75%. Furthermore, MD simulation was performed to explore stability and flexibility of residues at different positions. The average difference between the protein conformation and the original structure was measured using the root mean-square deviation (RMSD) [40]. From Figure 4C, the differences in the RMSD of St-2-2 and St-2-2 Δ C10 were small but the variant shows an overall decrease, revealing that St-2-2 Δ C10 was more stable during the simulation. The root-mean-square fluctuation (RMSF) is a valuable tool for describing local protein chain variations [40]. The rigidity of the active sites of Thr145-Tyr158-Lys162 were both stronger, and studies have shown that there is a positive correlation between the rigidity of the active site and the stability of enzymatic kinetics. Compared with WT, the flexibility of St-2-2 Δ C10 increased at loop 194–211 (Figure 4D). The C-terminal α -helix flexibility of St-2-2 was much higher. However, St-2-2 Δ C10 had a relatively rigid tail.

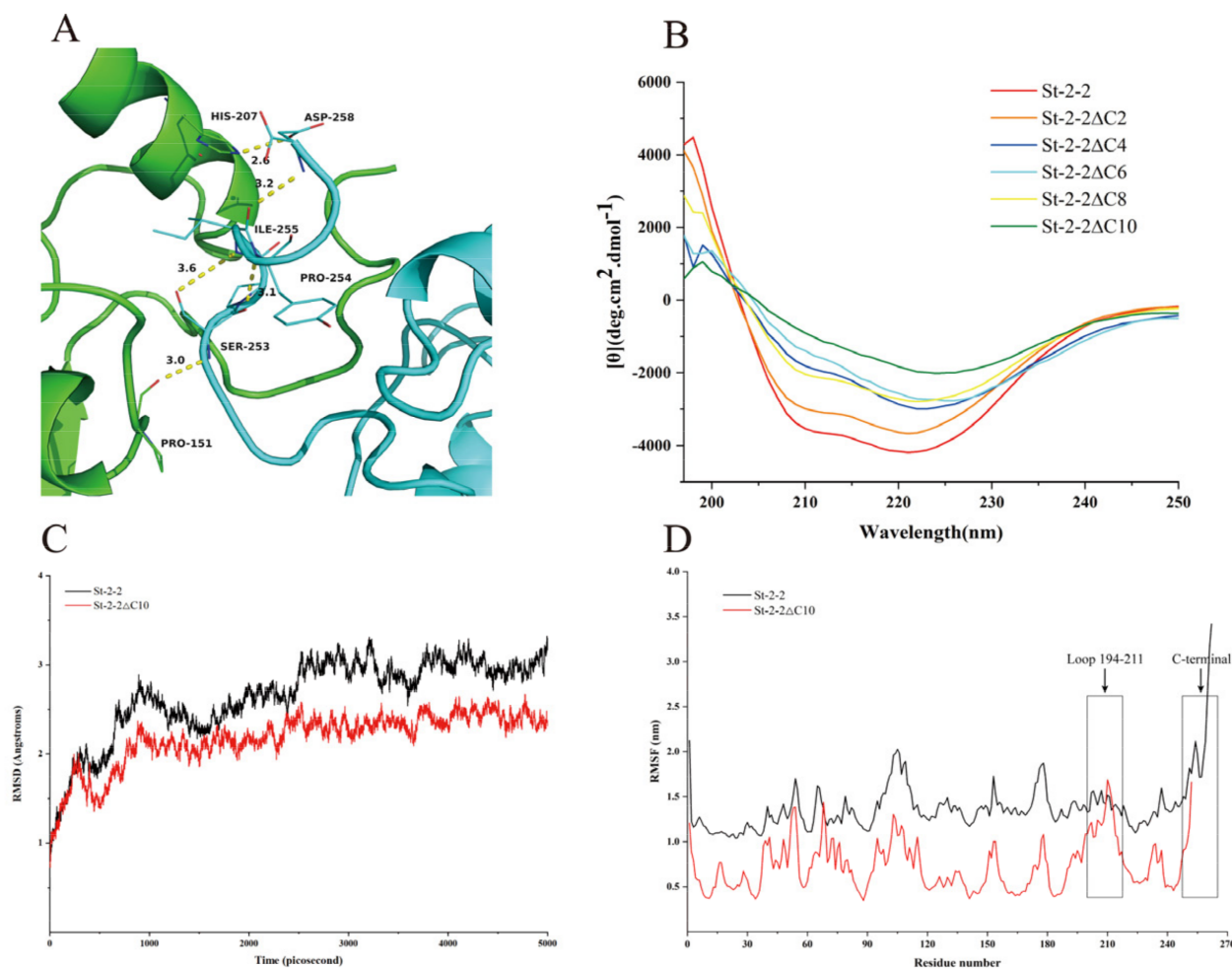


Figure 4. Structural analysis. (A) The interactions between the C-terminal of subunits in the diagonal position of St-2-2 tetrameric structure. (B) Far-UV CD spectra of St-2-2 and mutants. (C) RMSD and (D) RMSF computed from MD simulations for St-2-2 and St-2-2ΔC10.

The electrostatic surface charge distribution displayed that the substrate-binding site was hydrophobic (Figure 5A). The seven β -strand structures in parallel constituted the core of the molecule. They were in the same direction and their endpoints were almost on the same plane. β A, β B, β C, β D, β E, and β F formed the bottom of the active pocket. α E, α F, α G, and the short coil between them formed a loop structure, which together constituted a sidewall of the active pocket. Compared with the folded structure, the coiled structure was more susceptible to interaction between the side chains. The active site of St-2-2 and St-2-2ΔC10 was composed of the coiled structure (Figure 5A,B). The strongly hydrophilic region of St-2-2 was 69–70 (Figure 5C), and the strongly hydrophobic regions were concentrated at 17–24, 224–230 (Figure 5D). In St-2-2, the hydrophobic amino acid in the tail was not conducive to stability [26]. In St-2-2ΔC10, the loop in the C-terminal, α E– α F, and α G formed a hydrophilic surface. The results showed that enhanced surface hydrophilicity might influence entry and exit and St-2-2ΔC10 was more stable.

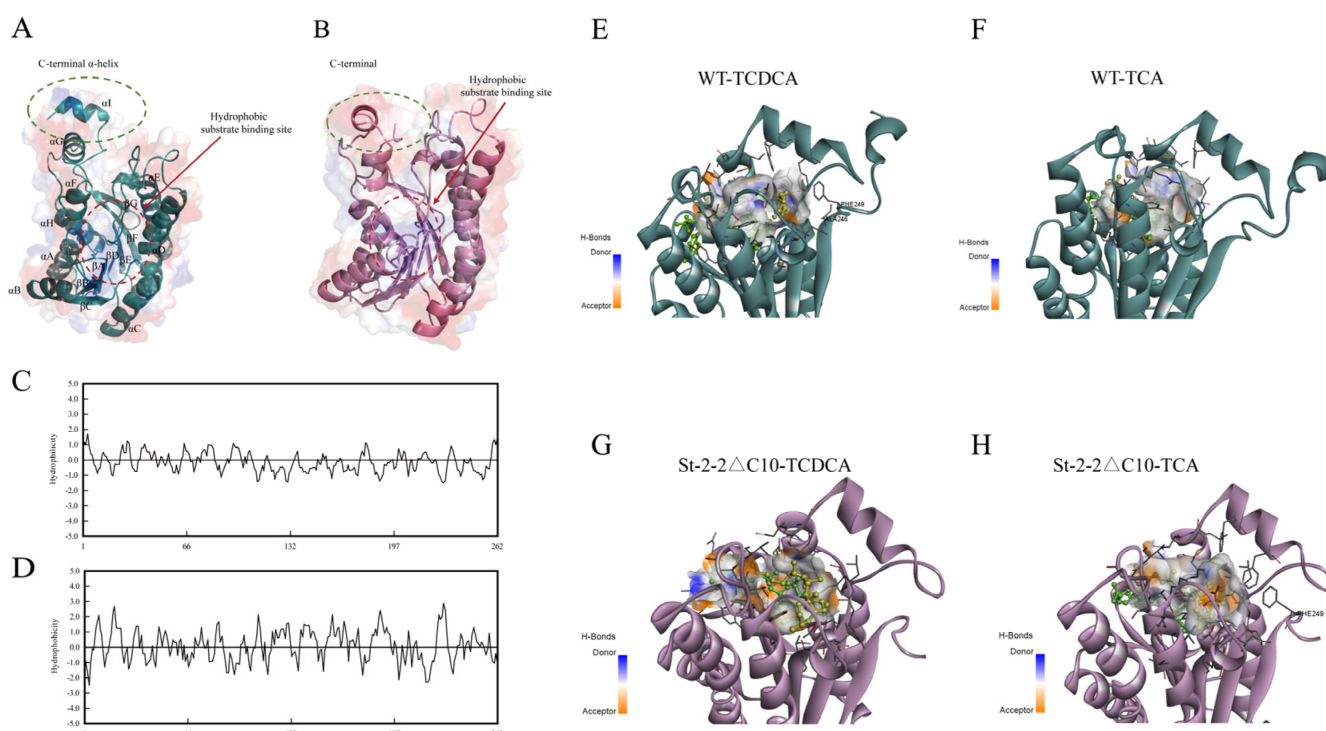


Figure 5. Structural analysis. Electrostatic charge surface view of (A) St-2-2 and (B) St-2-2 Δ C10. (C) St-2-2 hydrophilic analysis. (D) St-2-2 hydrophobicity analysis. Analysis of C-terminal interactions with substrates of (E) WT-TCDCA-NADP⁺ complex, (F) WT-TCA-NADP⁺ complex, (G) St-2-2 Δ C10-TCDCA-NADP⁺ complex, (H) St-2-2 Δ C10-TCA-NADP⁺ complex based on docking. TCDCA and TCA are colored in yellow sticks. NADP⁺ is colored in green sticks. WT and St-2-2 Δ C10 are colored in cyan and pink, respectively. The H-bond interaction of receptor surfaces is displayed as surface and the residues are colored by elements.

To further explore the reasons for substrate specificity, the changes in C-terminal amino acids were observed by molecular docking. From Figure 5E,F, the Phe249 of the C-terminal loop in the WT-NADP⁺-TCDCA ternary complex covered the active pocket and formed hydrophobic interactions with the substrate, but not in WT-NADP⁺-TCA. The catalytic activity of WT towards TCA was 2.1 times higher than that of TCDCA. In contrast, the Phe249 of the C-terminal loop reappeared in St-2-2 Δ C10-NADP⁺-TCA but disappeared in St-2-2 Δ C10-NADP⁺-TCDCA (Figure 5G,H). St-2-2 Δ C10 had no activity on TCA, activity on TCDCA, which still remained at 14.19 U/mg. There were not only changes in the C-terminal Phe249, but also a different conformational flip of NADP⁺ and change in the distance between the carbon on the benzene ring and Phe208 was observed. The distance between WT-TCDCA and Phe208 was 3.2 Å (Figure S3A), while the distance between St-2-2 Δ C10-TCDCA and Phe208 was 4.4 Å (Figure S3C). Similarly, the distance between St-2-2 Δ C10-TCA and Phe208 was reduced from 5.5 Å to 3.7 Å (Figure S3B,D), which greatly affected the entry of TCA into the active pocket, making St-2-2 Δ C10 retain catalytic activity only towards TCDCA.

2.7. Verification of the C-Terminal Truncation Strategy on Other 7α -HSDHs

To evaluate the C-terminal truncation strategy for altering substrate selectivity, the same method was implemented in two other 7α -HSDHs (J-1-1 and S1-a-1). J-1-1 [41] and S1-a-1 [38] originated from the gut microbiota of black bears, which share 66.79%, 59.93% amino acid sequence identities with St-2-2, respectively. As shown in Figure 3A, J-1-1 Δ C6 completely lost catalytic activities on TCA and GCA but remained active on TCDCA, GCDCA of 18.45 U/mg and 15.32 U/mg, respectively. Similarly, S1-a-1 Δ C8 also completely lost activities on TCA and GCA but remained active on TCDCA and GCDCA of 24.49 U/mg and

11.83 U/mg, respectively (Figure 3C). The catalytic efficiency (k_{cat}/K_m) of J-1-1 Δ C6, S1-a-1 Δ C8 remained 0.56%, 0.68% of wild enzymes, respectively (Table 1). No doubt, the C-terminal truncation of J-1-1 and S1-a-1 resulted in a complete substrate selectivity on TCDCA and GCDCA, which was consistent with the result of St-2-2. These encouraging results suggested that the C-terminal truncation strategy could be feasible for other 7 α -HSDHs to create new 7 α -HSDH variants for altering substrate selectivity.

2.8. Application for Selective Production of TUDCA from Waste Chicken Bile Powder

The asymmetric oxidization of 7 α -OH catalyzed by St-2-2 and St-2-2 Δ C10 combined with a 7 β -HSDH in a one-pot cascade was performed on a 50-mL scale to verify feasibility of selective production of TUDCA from waste chicken bile powder. The composition of reaction products was analyzed by HPLC-ELSD, and the standard curve is shown in Figure S4. As shown in Table 2, TCDCA conversion reached 84.23% and TUDCA yield reached 35.34%, catalyzed by St-2-2 Δ C10, which were slightly higher than that of St-2-2 (79.92%, 31.25%). In addition, from Figure 6, TUCA was not produced using St-2-2 Δ C10 for catalysis, while there was a clear TUCA peak at about 17 min using wild-type St-2-2 for catalysis.

Table 2. The TUDCA preparation results based on different enzymes.

	TCDCA Conversion ^b (%)	TUDCA Yield (%)	The Proportion of TUDCA in Total Bile Acid (%)
St-2-2	79.93	31.25	25.08
St-2-2 Δ C10	84.23	35.34	26.15

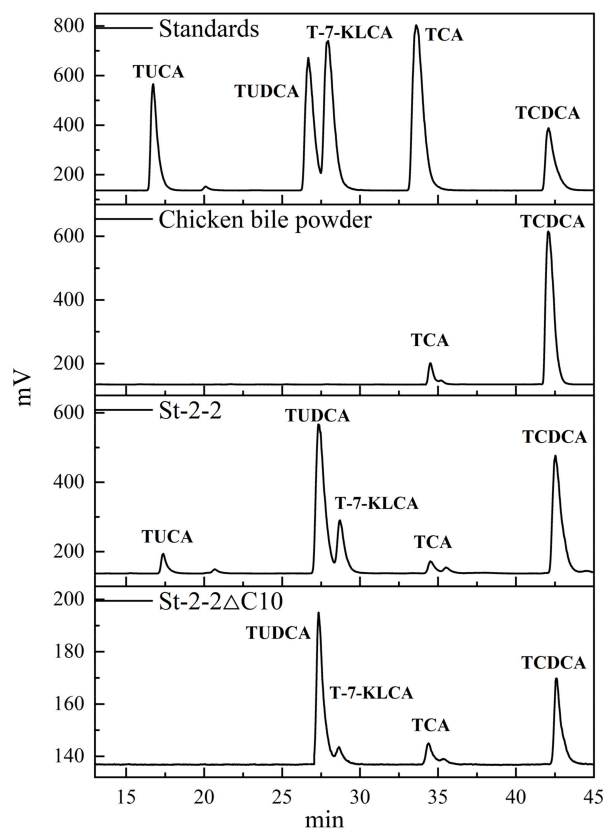


Figure 6. Products were analyzed by HPLC-ELSD. HPLC profile of TUCA, TUDCA, T-7-KLCA, TCA, and TCDCA; Chicken bile powder; Biosynthesis of TUDCA from waste chicken bile powder using St-2-2 as the catalyst; Selective biosynthesis of TUDCA from waste chicken bile powder using St-2-2 Δ C10 as the catalyst.

3. Discussion

Asymmetric reduction of carbonyl groups has been one of the hot spots in chemical reaction research [42]. As a class of oxidoreductases, hydroxysteroid dehydrogenases have strict stereoselectivity and a wide spectrum of substrates, and HSDH can catalyze asymmetric reduction of carbonyl groups, not only for steroids, but also for alkyl-substituted monocyclic ketones and dicyclic ketones [13]. Among them, the catalytic activity of 7α -HSDH for different steroids also varies greatly. 7α -HSDH from *Clostridium difficile* has a catalytic activity of 160 U/mg for CA and 8.5 U/mg for CDCA [43]; 7α -HSDH from *Escherichia coli* HB101 has a catalytic activity of 268 U/mg for CA and 190 U/mg for CDCA [44]; 7α -HSDH from *Xanthomonas maltophilia* has a catalytic activity of 70 U/mg for CA and the catalytic activity for CDCA was not reported [45]. 7α -HSDH in higher catalytic activity is more conducive to industrial application. In previous studies, researchers have aimed to improve the activity and thermostability of 7α -HSDHs, using mutagenesis and computational methods [21]. However, the effect of mutating 7α -HSDH on the catalytic activity of different substrates has still not been reported. To identify the key sites of 7α -HSDH for the catalytic activity of different substrates, we implemented a systematic strategy to analyze the conserved sites of known 7α -HSDHs by multiple sequence alignment, selected an additional α -helix structure at the C-terminal of St-2-2 by homology modeling and structural analysis, and then performed C-terminal truncation to investigate the effect of the tail on the entry and exit of different substrates, and, thus, effected the catalytic activity of different substrates.

Based on sequence and structural analysis, we deleted C-terminal amino acids of St-2-2. Interestingly, mutant St-2- Δ C10 only performed activities on TCDCA, but without activities on TCA. In contrast, the catalytic activities of WT on TCA (269.39 U/mg) was higher than on TCDCA (128.13 U/mg). The inversion of the catalytic activity of different substrates was achieved. The k_{cat} of St-2- Δ C10 decreased, which was possibly due to the change of the C-terminal loop above the substrate-binding pocket. The K_m value of St-2- Δ C10 showed a significant increase and the change in K_m was related to affinity for the substrate or cofactor [46].

Moreover, St-2-2 is a tetramer, and there are interactions between different subunits [28]. Yang et al. [47] obtained I31T/Q59T/I195Q through combinatorial mutation between subunits and within subunits, and the catalytic activity for aromatic aldehydes was increased by 278 times. The interface flexibility between different subunits was enhanced, substrate-binding pockets were enlarged, and proton transfer was improved. Interactions between different subunits of St-2-2 decrease with truncation of C-terminal. Therefore, the hydrogen bond interactions between different subunits of St-2-2 may have a certain impact on the catalytic activity. Besides this, the secondary structure influences the flexibility of the protein [48]. The α -helix at C-terminal of St-2- Δ C10 was completely lost and the content of α -helix reduced by 28.84%. The α -helix is the main structure that constitutes the flexibility of the enzyme [49]. The truncation of the C-terminal amino acid increased the stiffness of the protein and improved C-terminal rigidity might affect the entry and exit of substrates.

RMSD revealed that St-2- Δ C10 was more stable. The result was consistent with the hydrophilic analysis. Hydrophobicity reflects the folding of proteins and plays an important role in maintaining the tertiary structure of proteins. Optimizing the distribution of electrostatic charges on enzyme surface is a strategy to improve thermostability [50]. The C-terminal of St-2-2 is hydrophobic. In contrast, the loop in the C-terminal, α E- α F, and α G form a hydrophilic surface in St-2- Δ C10. Arabnejad et al. [51] designed a residue mutation at position 190 (E190T) on the surface of halohydrin dehalogenase, which experienced T_m value increase of 1.5 °C. E190T redistributed surface charges and improved interactions between subunits. Li et al. [52] found that increased hydrophobicity of the entrance tunnel and the altered shape of the binding pocket led to the change of catalytic profile. Therefore, enhanced surface hydrophilicity may influence entry and exit, and St-2- Δ C10 is more stable. From RMSF, St-2- Δ C10 had a flexible loop 194-211 and a relatively rigid tail. This might weaken the protein's encapsulation effect on the substrate so that a substrate with a

certain structure cannot be combined with the protein, that is, the phenomenon of substrate selectivity occurs. Similarly, Lou et al. [53] showed that the loop structure in CA 7 α -HSDH might contain favored candidate sites for enhancing thermostability. Zheng et al. [54] showed that the T189V/V207M mutation located in loops of *Rm* 7 β -HSDH had a specific activity 5.5-fold higher than those of WT. Tanaka et al. [55] found the C-terminal substrate-binding long loop containing the FG1 and FG2 helices underwent a large induced-fit movement upon binding to the substrate.

The results of molecular docking further showed that Phe249 covered the active pocket and formed hydrophobic interactions with the substrate. Phe249 might affect the entry and exit of the substrate and, thus, affect the catalytic activity. Similarly, in the apo *Eco*-7 α -HSDH structure, the Leu254 residue in the C-terminal loop formed hydrophobic interactions with the α 5- α 6 and α 8-helix regions. The substrate-binding site was capped and covered by the β 4- α 4 loop or C-terminal loop, which both prohibited nonspecific hydrophobic molecules from entering the substrate-binding site [26]. What was more, the decreased distance from Phe208 was unfavorable for the correct orientation of the substrate NADP⁺ to prevent the tail wobble from affecting the entry and exit of TCA into the active pocket [19]. As a result, St-2-2 Δ C10 specifically catalyzed TCDCA in chicken bile powder.

From HPLC-ELSD, there was no peak of TUCA. TUCA, as the by-product of the reaction increased the difficulty of separation, reduced the purity of the product, and was transformed into DCA in the body, causing the risk of colorectal cancer [56,57]. The results indicated that St-2-2 Δ C10 could be used in the application for selective production of TUDCA from waste chicken bile powder.

4. Materials & Methods

4.1. Chemicals and Materials

NADP⁺ was produced by Roche (Basel, Switzerland). PrimerSTAR Max DNA Polymerase, *Bam*HI, *Xho*I, and T4 DNA ligase were purchased from Takara (Dalian, China). *E. coli* DH5 α used for cloning and BL21 (DE3) served as a general host for protein expression were obtained from TransGen Biotech (Beijing, China). TCDCA, GCDCA, TCA, and GCA were obtained from the National Institutes for Food and Drug Control (Beijing, China). The chicken bile powder was donated by Shanghai Kaibao Pharmaceutical Co., Ltd., and the content of TCDCA is 55.1% (Shanghai, China).

4.2. Molecular Cloning

The 7 α -HSDH gene (St-2-2) was obtained via standard PCR techniques from black bear intestinal microbe metagenomic DNA (Accession number: SRP079591). Primers with recognition sites *Bam*HI and *Xho*I were used for amplification (for: 5'-CGCGGATCCATGAAAAGAGTAGAAAATAAAGTAG-3' and rev: 5'-CCGCTCGAGTTAAACAGCATCCCCATAAATAG-3'). The created *Bam*HI and *Xho*I fragment was recombined with the pGEX-6p-2 vector, then incubated overnight at 16 °C in the presence of T4 DNA ligase. The recombinant genes were transformed into *E. coli* DH5 α , plated on LB-agar plus ampicillin (50 μ g/mL) and verified by sequencing.

4.3. Mutation Design and Truncated Mutagenesis

The proposed C-terminal truncation strategy involved three steps. Firstly, multiple sequence alignments were used to identify the consensus sequence. Secondly, structural alignment was performed to detect unique similarities and differences among related proteins. Finally, potential sites in the C-terminal were identified, based on the conserved sequence and structural alignment information. Five truncated mutants of St-2-2 with C-terminal 2, 4, 6, 8, and 10 amino acids deleted were generated by the PCR method (primers listed in Table S1).

4.4. Expression and Purification of Recombinant Proteins

The recombinant genes were transformed into *E. coli* BL21 (DE3) for heterologous expression and purified by GST column (GE Healthcare). To identify enzyme expression and purity, sodium dodecyl sulfate-polyacrylamide gel electrophoresis (SDS-PAGE, Bio-Rad, Richmond, CA, USA) was used. Protein concentrations were determined by Pierce[®] BCA protein assay kit (Thermo Fisher Scientific, Waltham, MA, USA) according to instructions. Relative molecular mass was determined by gel filtration performed on ÄKTA[™] prime Plus (General electric medical system (China) Co., Ltd., Shanghai, China) according to the method reported previously [29]. The molecular mass of St-2-2 was also determined by matrix-assisted laser desorption ionization-time of flight mass spectrometry (MALDI-TOF-MS, MALDI-7090, Shimadzu Corporation, Kyoto, Japan) using SA as a matrix.

4.5. Phylogenetic Analysis and Sequence Alignment

A phylogenetic tree of St-2-2, the other known nine 7 α -HSDHs, and six 7 α -HSDHs from our previous work was constructed using MEGA7. Sequence alignment of these proteins was carried out on DNAMAN software v.6 (<http://www.biologydir.com/dnaman-info-1940.html>, accessed on 14 April 2020).

4.6. Enzymatic Activity and Kinetic Analysis

The standard reaction mixture contained Glycine-NaOH (50 mM, pH 10.0), NADP⁺ (0.5 mM), TCDCA (0.5 mM), and enzyme (2 μ g) in a final volume of 2 mL. The reaction was monitored for 30 s changes in absorbance of NADPH at 340 nm and 25 °C [53]. The kinetic parameters (K_m and V_{max}) of St-2-2 and its mutants were determined at different TCDCA concentrations (0.1–10 mM) under standard conditions and calculated by the Michaelis-Menten equation using nonlinear regression with GraphPad Prism 7.0 software (GraphPad Software, San Diego, CA, USA). All experiments were carried out three times.

4.7. Effects of pH and Temperature on Enzyme Activity and Stability

The optimum pH for St-2-2 was measured at different pH buffer including sodium phosphate buffer (50 mM, pH 5.0–8.0), Tris-HCl (50 mM, pH 8.0–9.0), and Glycine-NaOH (50 mM, pH 9.0–12.0), TCDCA (0.5 mM), NADP⁺ (0.5 mM), and enzyme (2 μ g). The influence of temperature on enzyme activity was investigated between 10 °C and 50 °C using TCDCA as substrate, Glycine-NaOH (50 mM, pH 10.0) as buffer, and reacted for 30 min. The thermal stability of St-2-2 was determined at different temperatures. The enzyme was incubated at 4 °C, 25 °C, 37 °C, and 50 °C, with TCDCA (0.5 mM) as the substrate, NADP⁺ (0.5 mM) as the coenzyme, and Glycine-NaOH (50 mM, pH 10.0), as the buffer solution. The enzymatic activity was measured under standard conditions.

4.8. Circular Dichroism (CD) Spectroscopy Measurements

The circular dichroism (CD) spectra of St-2-2 and mutants (0.2 mg/mL) were recorded at room temperature using Chirascan V100 Circular Dichroism Spectrometers (Applied Photophysics, Leatherhead, UK) equipped with a 1 mm path length cell. Each spectrum was the average of 10 scans with a bandwidth of 0.1 nm, a step resolution of 0.1 nm, and a scan rate of 1 nm/s. The data was collected from 195 to 250 nm.

4.9. Homology Alignment, Structure Modeling, Molecular Docking, and MD Simulation

The three-dimensional structures of St-2-2 and its mutants were generated by homology modeling of SWISS-MODEL online server (<https://swissmodel.expasy.org/>, accessed on 2 January 2021) and the I-TASSER server (<https://zhanglab.ccmb.med.umich.edu>, accessed on 13 January 2021). Docking of protein with ligand was implemented by Discovery studio 2016 software (Accelrys Software, Inc., San Diego, CA, USA). MD simulations were performed using Amber Molecular Dynamics Package (AMBER12). The system was built in TIP3 water box. After adding Na⁺ ions to neutralize the system's negative charges, the LEaP module generated topology and coordinate data. The energy was minimized with

the steepest descent algorithm for 10,000 steps. Further dynamics were simulated for 5 ns, heating the system to 300 K within 50 ps MD simulation [39].

4.10. Practical Preparation of TUDCA from Waste Chicken Bile Powder Using St-2-2 and St-2-2 Δ C10

TUDCA was prepared by using wild enzyme St-2-2 and its substrate selectivity mutant (St-2-2 Δ C10) combined with 7 β -HSDH from *C. absonum* ATCC27555 (GenBank: JN191345) in a 50-mL scale to evaluate the feasibility of the biocatalytic process. The reaction contained 50 mM Gly-NaOH, pH 10.0, chicken bile powder (equal to 8 mM TCDCA), NADP⁺ (2 mM), 7 α -HSDH (2.5 mg), 7 β -HSDH (7.5 mg) and was incubated at 25 °C for 4 h. The products were analyzed by HPLC-ELSD (Welch Ultimate XB-C18, 4.6 × 250 mm, 5 μ m, Agilent Technologies, Santa Clara, CA, USA). The products were separated by a silica gel column (40 × 300 mm), eluted using petroleum ether and ethyl acetate, and the samples were collected after rotary evaporation. ¹H NMR and ¹³C NMR were measured on 400 MHz NMR Spectrometer (DD2 400-MR, Agilent Technologies, Santa Clara, CA, USA).

5. Conclusions

In summary, we successfully expressed, characterized, and altered the substrate selectivity of St-2-2. The C-terminal truncation strategy could be extended to other 7 α -HSDHs, which would provide a good platform for the rational modification of hydroxysteroid dehydrogenases. Enhanced surface hydrophilicity and improved C-terminal rigidity affected the entry and exit of substrates. Hydrogen bond interaction between different subunits and interaction changes in Phe249 of the C-terminal loop inverted the substrate catalytic activity. This is the first study reporting the substrate selectivity of 7 α -HSDH. The finding that 7 α -HSDH specifically catalyzes TCDCA could not only be used in the catalysis of chicken bile powder but also to prepare bear bile powder, turning waste into treasure. It could also be applied to the quantitative determination of serum CDCA-conjugated bile acids.

Supplementary Materials: The following supporting information can be downloaded at: <https://www.mdpi.com/article/10.3390/catal12070781/s1>, Figure S1. The metabolic pathway of TUDCA in vivo; Figure S2. Structural comparison of 7 α -HSDHs; Figure S3. Reaction mechanism for the reduction of TCDCA to T-7-KLCA by 7 α -HSDH and the role of T-Y-K residues at the catalytic center; Figure S4. Interaction analysis of substrate and amino acid residues at C-terminal; Figure S5. HPLC calibration diagram; Figure S6. ¹H NMR of TUDCA prepared by enzymatic cascade reaction; Figure S7. ¹³C NMR of TUDCA prepared by enzymatic cascade reaction; Table S1: Primers used for mutagenesis.

Author Contributions: Conceptualization, Y.P. and S.T.; Methodology, Y.P. and S.T.; Software, Y.P.; Investigation, Y.P., S.T. and M.Z.; Data curation, Y.P. and F.A.; Writing—original draft preparation, Y.P.; Writing—review and editing, Y.P., Z.T., D.L., J.T. and L.Z.; Funding acquisition, B.W. All authors have read and agreed to the published version of the manuscript.

Funding: This work was supported by National Science and Technology Major Projects for “Major New Drugs Innovation and Development” (2017ZX09309-006), Chongqing Professional Talents Plan for Innovation and Entrepreneurship Demonstration Team (CQCY201903258).

Data Availability Statement: All data are included in this manuscript or the Supplementary Materials. Requests for data and materials should be addressed to Liancai Zhu and Bochu Wang.

Conflicts of Interest: The authors declare that there are no conflict of interest, and that no ethical approval was required for this work.

Abbreviations

7 α -HSDH	7 α -hydroxysteroid dehydrogenase
GCA	glycocholic acid
GCDCA	glycochenodeoxycholic acid
TUDCA	tauroursodeoxycholic acid
TCA	taurocholic acid
TUCA	taurourschocholic acid
TCDCA	taurochenodeoxycholic acid
UDCA	ursodeoxycholic acid
T-7-KLCA	taurine-7-ketolithocholic acid

References

1. Tabrizian, K.; Shahramian, I.; Bazi, A.; Afshari, M.; Ghaemi, A. Alleviating Effects of Ursodeoxycholic Acid in Children with Acute Hepatitis A Infection: A Randomized Clinical Trial. *Hepat. Mon.* **2019**, *19*, e86719. [[CrossRef](#)]
2. Suraweera, D.; Rahal, H.; Jimenez, M.; Viramontes, M.; Choi, G.; Saab, S. Treatment of primary biliary cholangitis ursodeoxycholic acid non-responders: A systematic review. *Liver Int.* **2017**, *37*, 1877–1886. [[CrossRef](#)] [[PubMed](#)]
3. Crosignani, A.; Battezzati, P.M.; Setchell, K.D.R.; Invernizzi, P.; Covini, G.; Zuin, M.; Podda, M. Tauroursodeoxycholic Acid for Treatment of Primary Biliary Cirrhosis: A Dose-Response Study. *Dig. Dis. Sci.* **1996**, *41*, 809–815. [[CrossRef](#)] [[PubMed](#)]
4. Tonin, F.; Arends, I.W.C.E. Latest development in the synthesis of ursodeoxycholic acid (UDCA): A critical review. *Beilstein J. Org. Chem.* **2018**, *14*, 470–483. [[CrossRef](#)]
5. Momose, T.; Tsubaki, T.; Iida, T.; Nambara, T. An improved synthesis of taurine- and glycine-conjugated bile acids. *Lipids* **1997**, *32*, 775–778. [[CrossRef](#)]
6. Chiang, J.Y.L. Bile acid metabolism and signaling in liver disease and therapy. *Liver Res.* **2017**, *1*, 3–9. [[CrossRef](#)]
7. Fedorowski, T.; Salen, G.; Tint, G.S.; Mosbach, E. Transformation of Chenodeoxycholic Acid and Ursodeoxycholic Acid by Human Intestinal Bacteria. *Gastroenterology* **1979**, *77*, 1068–1073. [[CrossRef](#)]
8. Lepercq, P.; Gérard, P.; Béguet, F.; Grill, J.-P.; Relano, P.; Cayuela, C.; Juste, C. Isolates from normal human intestinal flora but not lactic acid bacteria exhibit 7 α - and 7 β -hydroxysteroid dehydrogenase activities. *Microb. Ecol. Health Dis.* **2004**, *16*, 195–201. [[CrossRef](#)]
9. Ferrandi, E.E.; Bertolesi, G.M.; Polentini, F.; Negri, A.; Riva, S.; Monti, D. In search of sustainable chemical processes: Cloning, recombinant expression, and functional characterization of the 7 α - and 7 β -hydroxysteroid dehydrogenases from *Clostridium absonum*. *Appl. Microbiol. Biotechnol.* **2012**, *95*, 1221–1233. [[CrossRef](#)]
10. Ridlon, J.M.; Kang, D.-J.; Hylemon, P.B. Bile salt biotransformations by human intestinal bacteria. *J. Lipid Res.* **2006**, *47*, 241–259. [[CrossRef](#)]
11. Ji, Q.; Wang, B.; Li, C.; Hao, J.; Feng, W. Co-immobilised 7 α - and 7 β -HSDH as recyclable biocatalyst: High-performance production of TUDCA from waste chicken bile. *RSC Adv.* **2018**, *8*, 34192–34201. [[CrossRef](#)]
12. Wang, Y.; Wu, C.; Lu, D. Determination of bear bile acids in Fel Ursi and chick gall, duck gall and dog gall by capillary electrophoresis. *Strait Pharm. J.* **2006**, *18*, 61–63.
13. Graff, M.; Buchholz, P.C.F.; Stockinger, P.; Bommarius, B.; Bommarius, A.S.; Pleiss, J. The Short-Chain Dehydrogenase/Reductase Engineering Database (SDRED): A classification and analysis system for a highly diverse enzyme family. *Proteins* **2019**, *87*, 443–451. [[CrossRef](#)]
14. Sun, Y.; Calderini, E.; Kourist, R. A Reconstructed Common Ancestor of the Fatty Acid Photo-decarboxylase Clade Shows Photo-decarboxylation Activity and Increased Thermostability. *ChemBioChem* **2021**, *22*, 1833–1840. [[CrossRef](#)]
15. Cahn, J.K.; Werlang, C.A.; Baumschlager, A.; Brinkmann-Chen, S.; Mayo, S.L.; Arnold, F.H. A General Tool for Engineering the NAD/NADP Cofactor Preference of Oxidoreductases. *ACS Synth. Biol.* **2017**, *6*, 326–333. [[CrossRef](#)]
16. You, Z.N.; Chen, Q.; Shi, S.C.; Zheng, M.M.; Pan, J.; Qian, X.L.; Li, C.X.; Xu, J.H. Switching Cofactor Dependence of 7 β -Hydroxysteroid Dehydrogenase for Cost-Effective Production of Ursodeoxycholic Acid. *ACS Catalysis* **2019**, *9*, 466–473. [[CrossRef](#)]
17. Chen, Y.; Zhao, Y.; Zhou, X.; Liu, N.; Ming, D.; Zhu, L.; Jiang, L. Improving the thermostability of trehalose synthase from *Thermomonospora curvata* by covalent cyclization using peptide tags and investigation of the underlying molecular mechanism. *Int. J. Biol. Macromol.* **2021**, *168*, 13–21. [[CrossRef](#)]
18. Kim, S.H.; Park, S.; Park, E.; Kim, J.H.; Ghatge, S.; Hur, H.G.; Rhee, S. Structure and substrate specificity determinants of NfnB, a dinitroaniline herbicide-catabolizing nitroreductase from *Sphingopyxis* sp. strain HMH. *J. Biol. Chem.* **2021**, *297*, 101143. [[CrossRef](#)]
19. Kim, J.-S.; Patel, S.; Tiwari, M.; Lai, C.; Kumar, A.; Kim, Y.; Kalia, V.; Lee, J.-K. Phe-140 Determines the Catalytic Efficiency of Arylacetonitrilase from *Alcaligenes faecalis*. *Int. J. Mol. Sci.* **2020**, *21*, 7859. [[CrossRef](#)]
20. Gao, H.; Li, J.; Sivakumar, D.; Kim, T.-S.; Patel, S.K.S.; Kalia, V.C.; Kim, I.-W.; Zhang, Y.-W.; Lee, J.-K. NADH oxidase from *Lactobacillus reuteri*: A versatile enzyme for oxidized cofactor regeneration. *Int. J. Biol. Macromol.* **2019**, *123*, 629–636. [[CrossRef](#)]
21. Liu, Z.Y.; Zhang, R.Z.; Zhang, W.C.; Xu, Y. Ile258Met mutation of *Brucella melitensis* 7 α -hydroxysteroid dehydrogenase significantly enhances catalytic efficiency, cofactor affinity, and thermostability. *Appl. Microbiol. Biotechnol.* **2021**, *105*, 3573–3586. [[CrossRef](#)]

22. Huang, B.; Zhao, Q.; Zhou, J.H.; Xu, G. Enhanced activity and substrate tolerance of 7-hydroxysteroid dehydrogenase by directed evolution for 7-ketolithocholic acid production. *Appl. Microbiol. Biotechnol.* **2019**, *103*, 2665–2674. [[CrossRef](#)]
23. Dhagat, U.; Endo, S.; Mamiya, H.; Hara, A.; El-Kabbani, O. Studies on a Tyr residue critical for the binding of coenzyme and substrate in mouse 3(17)alpha-hydroxysteroid dehydrogenase (AKR1C21): Structure of the Y224D mutant enzyme. *Acta Crystallogr. Sect. D-Struct. Biol.* **2010**, *66*, 198–204. [[CrossRef](#)]
24. Dhagat, U.; Endo, S.; Soda, M.; Hara, A.; El-Kabbani, O. Factorizing the role of a critical leucine residue in the binding of substrate to human 20 alpha-hydroxysteroid dehydrogenase (AKR1C1): Molecular modeling and kinetic studies of the Leu308Val mutant enzyme. *Bioorg. Med. Chem. Lett.* **2010**, *20*, 5274–5276. [[CrossRef](#)]
25. Lou, D.; Wang, B.; Tan, J.; Zhu, L. Carboxyl-terminal and Arg38 are essential for activity of the 7 α -hydroxysteroid dehydrogenase from *Clostridium absonum*. *Protein Pept. Lett.* **2014**, *21*, 894–900. [[CrossRef](#)]
26. Kim, K.-H.; Lee, C.W.; Pardhe, B.D.; Hwang, J.; Do, H.; Lee, Y.M.; Lee, J.H.; Oh, T.-J. Crystal structure of an apo 7 α -hydroxysteroid dehydrogenase reveals key structural changes induced by substrate and co-factor binding. *J. Steroid Biochem. Mol. Biol.* **2021**, *212*, 105945. [[CrossRef](#)]
27. Pal, D.; Chakrabarti, P. Terminal residues in protein chains: Residue preference, conformation, and interaction. *Biopolymers* **2000**, *53*, 467–475. [[CrossRef](#)]
28. Lou, D.; Wang, B.; Tan, J.; Zhu, L.; Cen, X.; Ji, Q.; Wang, Y.J.S.R. The three-dimensional structure of *Clostridium absonum* 7 α -hydroxysteroid dehydrogenase: New insights into the conserved arginines for NADP(H) recognition. *Sci. Rep.* **2016**, *6*, 22885. [[CrossRef](#)]
29. Tang, S.; Pan, Y.; Lou, D.; Ji, S.; Zhu, L.; Tan, J.; Qi, N.; Yang, Q.; Zhang, Z.; Yang, B.; et al. Structural and functional characterization of a novel acidophilic 7 α -hydroxysteroid dehydrogenase. *Protein Sci.* **2019**, *28*, 910–919. [[CrossRef](#)]
30. Tonin, F.; Otten, L.G.; Arends, I. NAD(+)-Dependent Enzymatic Route for the Epimerization of Hydroxysteroids. *ChemSusChem.* **2019**, *12*, 3192–3203. [[CrossRef](#)] [[PubMed](#)]
31. Sebahia, M.; Wren, B.W.; Mullany, P.; Fairweather, N.F.; Minton, N.; Stabler, R.; Thomson, N.R.; Roberts, A.P.; Cerdeño-Tárraga, A.M.; Wang, H.; et al. The multidrug-resistant human pathogen *Clostridium difficile* has a highly mobile, mosaic genome. *Nat. Genet.* **2006**, *38*, 779–786. [[CrossRef](#)] [[PubMed](#)]
32. Coleman, J.P.; Hudson, L.L.; Adams, M.J. Characterization and regulation of the NADP-linked 7 alpha-hydroxysteroid dehydrogenase gene from *Clostridium sordellii*. *J. Bacteriol.* **1994**, *176*, 4865–4874. [[CrossRef](#)] [[PubMed](#)]
33. Winter, J.; Morris, G.N.; O'Rourke-Locascio, S.; Bokkenheuser, V.D.; Mosbach, E.H.; Cohen, B.I.; Hylemon, P.B. Mode of action of steroid desmolase and reductases synthesized by *Clostridium "scindens"* (formerly *Clostridium* strain 19). *J. Lipid Res.* **1984**, *25*, 1124–1131. [[CrossRef](#)]
34. Baron, S.F.; Franklund, C.V.; Hylemon, P.B. Cloning, sequencing, and expression of the gene coding for bile acid 7 alpha-hydroxysteroid dehydrogenase from *Eubacterium* sp. strain VPI 12708. *J. Bacteriol.* **1991**, *173*, 4558–4569. [[CrossRef](#)]
35. Bennett, M.J.; McKnight, S.L.; Coleman, J.P. Cloning and characterization of the NAD-dependent 7alpha-Hydroxysteroid dehydrogenase from *Bacteroides fragilis*. *Curr. Microbiol.* **2003**, *47*, 475–484. [[CrossRef](#)]
36. Leopold, S.R.; Magrini, V.; Holt, N.J.; Shaikh, N.; Mardis, E.R.; Cagno, J.; Ogura, Y.; Iguchi, A.; Hayashi, T.; Mellmann, A.; et al. A precise reconstruction of the emergence and constrained radiations of *Escherichia coli* O157 portrayed by backbone concatenomic analysis. *Proc. Natl. Acad. Sci. USA* **2009**, *106*, 8713–8718. [[CrossRef](#)]
37. Filling, C.; Berndt, K.D.; Benach, J.; Knapp, S.; Prozorovski, T.; Nordling, E.; Ladenstein, R.; Jornvall, H.; Oppermann, U. Critical residues for structure and catalysis in short-chain dehydrogenases/reductases. *J. Biol. Chem.* **2002**, *277*, 25677–25684. [[CrossRef](#)]
38. Song, C.; Wang, B.; Tan, J.; Zhu, L.; Lou, D. Discovery of tauroursodeoxycholic acid biotransformation enzymes from the gut microbiome of black bears using metagenomics. *Sci. Rep.* **2017**, *7*, 45495. [[CrossRef](#)]
39. Lou, D.; Wang, Y.; Tan, J.; Zhu, L.; Ji, S.; Wang, B. Functional contribution of coenzyme specificity-determining sites of 7 α -hydroxysteroid dehydrogenase from *Clostridium absonum*. *Comput. Biol. Chem.* **2017**, *70*, 89–95. [[CrossRef](#)]
40. Martínez, L. Automatic identification of mobile and rigid substructures in molecular dynamics simulations and fractional structural fluctuation analysis. *PLoS ONE* **2015**, *10*, e0119264. [[CrossRef](#)]
41. Ji, S.; Pan, Y.; Zhu, L.; Tan, J.; Tang, S.; Yang, Q.; Zhang, Z.; Lou, D.; Wang, B. A novel 7 alpha-hydroxysteroid dehydrogenase: Magnesium ion significantly enhances its activity and thermostability. *Int. J. Biol. Macromol.* **2021**, *177*, 111–118. [[CrossRef](#)]
42. An, J.; Nie, Y.; Xu, Y. Structural insights into alcohol dehydrogenases catalyzing asymmetric reductions. *Crit. Rev. Biotechnol.* **2019**, *39*, 366–379. [[CrossRef](#)]
43. Bakonyi, D.; Hummel, W. Cloning, expression, and biochemical characterization of a novel NADP+-dependent 7 α -hydroxysteroid dehydrogenase from *Clostridium difficile* and its application for the oxidation of bile acids. *Enzyme Microb. Technol.* **2017**, *99*, 16–24. [[CrossRef](#)]
44. Yoshimoto, T.; Higashi, H.; Kanatani, A.; Lin, X.S.; Nagai, H.; Oyama, H.; Kurazono, K.; Tsuru, D. Cloning and sequencing of the 7 alpha-hydroxysteroid dehydrogenase gene from *Escherichia coli* HB101 and characterization of the expressed enzyme. *J. Bacteriol.* **1991**, *173*, 2173–2179. [[CrossRef](#)]
45. Pedrini, P.; Andreotti, E.; Guerrini, A.; Dean, M.; Fantin, G.; Giovannini, P.P. *Xanthomonas maltophilia* CBS 897.97 as a source of new 7 β - and 7 α -hydroxysteroid dehydrogenases and cholyglycine hydrolase: Improved biotransformations of bile acids. *Steroids* **2006**, *71*, 189–198. [[CrossRef](#)]

46. Lee, J.; Goodey, N.M. Catalytic Contributions from Remote Regions of Enzyme Structure. *Chem. Rev.* **2011**, *111*, 7595–7624. [[CrossRef](#)]
47. Yang, X.; Wu, L.; Li, A.; Ye, L.; Zhou, J.; Yu, H. The engineering of decameric d-fructose-6-phosphate aldolase a by combinatorial modulation of inter- and intra-subunit interactions. *Chem. Commun.* **2020**, *56*, 7561–7564. [[CrossRef](#)]
48. Martínez, D.; Cutiño-Avila, B.; Pérez, E.R.; Menéndez, C.; Hernández, L.; del Monte-Martínez, A. A thermostable exo- β -fructosidase immobilised through rational design. *Food Chem.* **2014**, *145*, 826–831. [[CrossRef](#)]
49. Ban, X.; Liu, Y.; Zhang, Y.; Gu, Z.; Li, C.; Cheng, L.; Hong, Y.; Dhoble, A.S.; Li, Z. Thermostabilization of a thermophilic 1,4-alpha-glucan branching enzyme through C-terminal truncation. *Int. J. Biol. Macromol.* **2018**, *107*, 1510–1518. [[CrossRef](#)]
50. Gribenko, A.V.; Patel, M.M.; Liu, J.; McCallum, S.A.; Wang, C.; Makhatadze, G.I. Rational stabilization of enzymes by computational redesign of surface charge-charge interactions. *Proc. Natl. Acad. Sci. USA* **2009**, *106*, 2601–2606. [[CrossRef](#)]
51. Arabnejad, H.; Dal Lago, M.; Jekel, P.A.; Floor, R.J.; Thunnissen, A.W.H.; Terwisscha van Scheltinga, A.C.; Wijma, H.J.; Janssen, D.B. A robust cosolvent-compatible halohydrin dehalogenase by computational library design. *Protein Eng. Des. Sel.* **2017**, *30*, 173–187. [[CrossRef](#)]
52. Li, G.Y.; Yao, P.Y.; Gong, R.; Li, J.L.; Liu, P.; Lonsdale, R.; Wu, Q.Q.; Lin, J.P.; Zhu, D.M.; Reetz, M.T. Simultaneous engineering of an enzyme's entrance tunnel and active site: The case of monoamine oxidase MAO-N. *Chem. Sci.* **2017**, *8*, 4093–4099. [[CrossRef](#)]
53. Lou, D.S.; Tan, J.; Zhu, L.C.; Ji, S.L.; Tang, S.J.; Yao, K.Y.; Han, J.X.; Wang, B.C. Engineering *Clostridium absonum* 7 alpha-hydroxysteroid Dehydrogenase for Enhancing Thermostability Based on Flexible Site and Delta Delta G Prediction. *Protein Pept. Lett.* **2018**, *25*, 230–235. [[CrossRef](#)]
54. Zheng, M.M.; Chen, K.C.; Wang, R.F.; Li, H.; Li, C.X.; Xu, J.H. Engineering 7 beta-Hydroxysteroid Dehydrogenase for Enhanced Ursodeoxycholic Acid Production by Multiobjective Directed Evolution. *J. Agric. Food Chem.* **2017**, *65*, 1178–1185. [[CrossRef](#)]
55. Tanaka, N.; Nonaka, T.; Tanabe, T.; Yoshimoto, T.; Tsuru, D.; Mitsui, Y. Crystal Structures of the Binary and Ternary Complexes of 7 α -Hydroxysteroid Dehydrogenase from *Escherichia coli*. *Biochemistry* **1996**, *35*, 7715–7730. [[CrossRef](#)]
56. Chaudhari, S.N.; Luo, J.N.; Harris, D.A.; Aliakbarian, H.; Yao, L.; Paik, D.; Subramaniam, R.; Adhikari, A.A.; Vernon, A.H.; Kiliç, A.; et al. A microbial metabolite remodels the gut-liver axis following bariatric surgery. *Cell Host Microbe.* **2021**, *29*, 408–424. [[CrossRef](#)]
57. Bernstein, C.; Holubec, H.; Bhattacharyya, A.K.; Nguyen, H.; Payne, C.M.; Zaitlin, B.; Bernstein, H. Carcinogenicity of deoxycholate, a secondary bile acid. *Arch. Toxicol.* **2011**, *85*, 863–871. [[CrossRef](#)]